Determination of Small Melt Fraction Peridotite Partial Melts Using Re Foil Melt Traps

A THESIS
SUBMITTED TO THE FACULTY OF THE GRADUATE SCHOOL
OF THE UNIVERSITY OF MINNESOTA
BY

Frederick Arthur Davis

IN PARTIAL FULFILLMENT OF THE REQUIREMENTS
FOR THE DEGREE OF
MASTER OF SCIENCE

Dr. Marc M. Hirschmann, Advisor

March, 2011

Abstract

The global record of trace element and isotopic compositions of ocean island basalts (OIB) suggest that they are derived from several distinct reservoirs in the mantle. Major and minor element compositions of OIB also span a relatively large range of compositions when compared with the more nearly uniform basaltic compositions erupted at mid-ocean ridges. This may be due to distinct melting lithologies or conditions of melting beneath different oceanic islands. The upper mantle is widely believed to be composed primarily of peridotite, which likely contributes to the formation of OIB. Melting at most OIB localities is confined to depths beneath the rigid oceanic lithosphere (~100 km) at pressures ~3 GPa where garnet is the stable aluminous phase, and the high incompatible element concentrations in these basalts suggest that melting is limited to low melt fractions. Thus, identifying the composition of low melt fraction partial melts of garnet peridotite at 3 GPa is key to understanding the genesis of OIB.

Low melt fraction partial melts of garnet peridotite were produced experimentally at 3 GPa in a piston cylinder apparatus using a new Re-foil melt trap. Melt traps allow partial melts to be segregated from crystalline residues, preventing changes in the compositions of small melt pools that can result from crystallization onto nearby mineral grains while the experiment is quenching. Re-foil melt traps are similar to diamond aggregate and vitreous carbon sphere traps, but rely upon the wetting properties of Re as well as pressure gradients to attract the melt phase. Re traps are easier to polish than diamond traps and, unlike vitreous carbon spheres, are capable of withstanding high temperatures required for peridotite partial melting at 3 GPa.

Partial melting experiments were performed in Pt/C capsules containing natural peridotite powder, KLB-1, or an oxide mixture approaching the composition of KLB-1. Experiments were performed from 1470-1530 °C and produced melt fractions between 0.059 and 0.235. In contrast with previous peridotite melting studies at 3 GPa, melts in the lowest melt fraction experiments coexisted with garnet. Resulting melt compositions are similar to those found by other peridotite partial melting studies for many components, including: TiO_2, Cr_2O_3, MnO, MgO, and Na_2O; however, there are relatively large differences in FeO* and CaO from the melt compositions of Walter (1998). FeO* in Re trap experiments varies from 6.6-7.9%, considerably lower than the Walter (1998) melts which are never lower than 8.8% FeO* at 3 GPa, and CaO varies from 11.4-14.3%, significantly higher than melts in Walter (1998) that vary from 7.7-10.9%.

The Re trap method successfully produces large melt pools that can be analyzed by electron microprobe at melt fractions as low as 0.05, although this may be about the lower limit of its effectiveness. The disagreements with previous experiments in CaO and FeO* contents are likely the result of the heterogeneous character of the melt pools and cast doubt on whether the measured compositions of melts produced in these experiments are true low-degree peridotite melt compositions.

Table of Contents

List of Tables

List of Figures

Introduction

It is widely accepted that ocean island basalts (OIB) are derived from low melt fraction partial melts of mantle material, but the lithology of the OIB source is still in question. Major and trace element compositions and isotopic ratios of mid-ocean ridge basalts (MORB), continental crust, and upper mantle peridotite fit together to describe a cohesive history of differentiation leading to the formation of these reservoirs from the primitive mantle (Hofmann, 1988), but the simplicity of the MORB-source mantle is not evident in the OIB system. OIBs vary greatly in major, minor, and trace element chemistry leading to many different suggestions as to their sources (e.g. Zindler and Hart, 1986). Important constraints on the sources of OIB are provided by experimental determination and characterization of partial melts of likely source lithologies.

Many studies of the trace element and isotope signatures of OIB have led to a widely accepted paradigm that mantle melts are derived from mixtures between a variety of distinct sources (e.g. Zindler and Hart, 1986; Hofmann, 1997). One such suggested OIB source is subducted oceanic crust (eclogite); the suggestion of eclogite was originally based on high levels of incompatible elements and both depleted and enriched isotopic signatures in OIB (Chase, 1981; Hofmann and White, 1982). There is also evidence that these isotopic signatures correlate with distinct major element trends in OIB, especially high SiO_2, which fit with addition of oceanic crust to the source (Hauri, 1996). Experiments have shown that moderate amounts (10-20%) of eclogite-derived melt could be present in some high-SiO_2 OIB (Johnston, 1986; Yasuda et al., 1994; Yaxley and Green, 1998; Takahashi and Nakajima, 2002; Pertermann and Hirschmann, 2003; Yaxley and Sobolev, 2007). Pyroxenite veins in the mantle may be a source of

alkalic OIB magmas. Garnet pyroxenite produces melts with similar CaO, FeO*, and SiO_2 contents to alkalic basalts but must form at high pressure (5 GPa) to contain sufficiently low Al_2O_3 (Hirschmann et al., 2003; Kogiso et al, 2003). Each of these sources may play an important role in the genesis of a particular subset of OIB, but it is hard to imagine any scenario where fertile mantle peridotite isn't an important component. While the variation in OIB may exceed that which can be explained by partial melting of peridotite, its presumed ubiquity in the mantle suggests that it must play some significant role in OIB genesis.

If dry peridotite melting can account for the major element compositions of some OIB, it will be at low extents of melting. Isotope studies have shown that OIB magmas have incompatible element abundances hundreds to thousands of times chondrite (e.g. Chauvel et al, 1992), which suggests they formed as low-degree partial melts. Low melt fraction (<0.2) peridotite partial melting experiments have been reported at relatively low pressures (1-2 GPa) in the spinel stability field (Hirose and Kushiro, 1993; Baker and Stolper, 1994; Pickering-Witter and Johnston, 2000; Wasylenki et al., 2003), but the record of peridotite partial melting experiments below a melt fraction of about 0.2 is impoverished at pressures relevant to OIB generation (~3 GPa).

3 GPa is the pressure at a depth of ~100 km, the average thickness of oceanic lithosphere and a likely depth of generation for many OIB. At this depth garnet is the stable aluminous phase instead of spinel. Significant changes in compositional trends may accompany the phase change. As demonstrated by Walter (1998) garnet is the first phase to be exhausted at 3 GPa, but no peridotite melts that equilibrated with garnet were

measured. Low melt fraction experiments will help to determine what effects garnet has on melt composition trends.

There are other properties of melts which may be better determined through direct observation than by modeling. Because the behavior of some incompatible elements cannot be accurately predicted by simple regressions, it is necessary to obtain these melts experimentally. For example, peridotite melts at low extents of melting contain more alkalis, which correlate with increased silica in the melt, and high TiO_2, which has the opposite effect (Hirschmann et al, 1998). Direct measurements will help to determine the concentrations of these incompatibles in low-degree peridotite melts and their effects on other major elements.

The partition coefficients determined from melting experiments are a fundamental part of mantle melting models. The model of Prytulak and Elliott (2007) is a recent example from the literature, which attempts to use TiO_2 concentrations in OIB to determine the extent of melting of the source region. They rely upon estimations of the TiO_2 content of small melt fraction peridotite melts from experiments at higher melt fraction to make their comparison. Direct experimental measurements will be able to improve models like these.

A large body of experimental work has focused on determining the compositions of peridotite partial melts. While it is relatively simple to perform these experiments at high melt fractions, low degree partial melts are more difficult to obtain. The simple melting experiments described in Walter (1998) provide a comprehensive dataset of peridotite partial melts over a large pressure and temperature range; however, straight-forward melting experiments like these cannot be used to explore melt fractions below

about 0.2. Modification of the experimental design is necessary to obtain measurable low-degree partial melts.

Partial melts in high pressure experimental capsules form melt pockets between mineral grains. These pockets become smaller in size as the melt fraction of an experiment decreases. One important implication is that at some small melt fraction the melt pocket will become too small to analyze with a microprobe beam. More important still are the effects of quench crystallization on the composition of the melt. During the quench phase of an experiment some crystallization will occur on surrounding olivine and pyroxene crystals, which are available as nucleation sites (Mysen and Kushiro, 1977). This disequilibrium crystallization can change the preserved composition of the quenched melt phase. Any experiment attempting to capture low melt fraction peridotite melts must be able to pool melts in large enough volumes for analysis and segregate the melt from crystalline phases either by trapping the melt or by forming pockets large enough to be unaffected by quench crystallization.

Two different methods have been used in previous studies to obtain this effect. Sandwich experiments attempt to put the peridotite into contact with basalt that approximates the expected melt composition and allow it to equilibrate with the peridotite mineral assemblage (Stolper, 1980; Takahashi and Kushiro, 1983; Falloon and Green, 1987). This method is problematic because it changes the composition of the solid as well as the melt and may not allow for complete equilibration. The experiments can also be performed iteratively (Robinson et al, 1998), using resultant liquid compositions for subsequent experiments. Even when the number of iterations is reduced by calculating

melt compositions from partitioning data (Hirschmann and Dasgupta, 2007), it takes many iterations and considerable effort to obtain even one melt composition.

For this reason it is tempting to design a melt trap to allow for melts at multiple melt fractions to be determined quickly. Melt traps form segregated pools of melt that are large enough to analyze. To be effective, they must also allow chemical communication between the pools and the residual minerals in the experimental charge. Ideally, the initial melt that enters the trap remains in chemical communication throughout the experiment and is able to equilibrate with the residue through diffusion.

In the past, diamond aggregates (Hirose and Kushiro, 1993; Baker and Stolper, 1994; Hirose, 1997b; Falloon et al, 1999), vitreous carbon spheres (Pickering-Witter and Johnston, 2000; Wasylenki et al, 2003; Pertermann and Hirschmann, 2003), and crimped Ag-Pd and Au-Pd inner capsules (Hirose and Kawamoto, 1995; Hirose, 1997a) have been employed as melt traps in peridotite partial melting experiments. These methods are hampered by the formation of low pressure zones (Falloon et al, 1996) and, for diamonds, by difficulties in polishing the run products. The traps work by creating a pressure gradient in the capsule. The melt is drawn into the low pressure zone and resides there for the rest of the run. The pressure gradient may cause the melt to exist at a pressure different from the nominal pressure of the run, so that even if the melt is in chemical communication with the residue, it may not represent equilibrium pressure conditions. It is also difficult to polish through diamond aggregate, and if the glass is removed from the trap for analysis (Baker and Stolper, 1994) contextual information is lost. Vitreous carbon spheres have been a useful melt trap material in partial melting experiments at the relatively low pressures associated with mid-ocean ridge melting (Pickering-Witter and

Johnston, 2000; Wasylenki et al, 2003). However, these are not useful at 3 GPa because they devitrify bove 1400° C, well below the peridotite solidus at 3 GPa (Kogiso and Hirschmann, 2001). LaPorte et al (2004) attempted to measure melts segregated in microdikes, melt-filled cracks in the graphite inner capsule, but microdikes do not occur consistently in graphite inner capsules.

In this study we test a new type of melt trap made of pieces of rhenium foil that can be used at high pressures and can be polished more easily than diamonds. The Re trap design was inspired by a phenomenon observed in a hydrous basalt melting experiment using a Re capsule. In that experiment, it was observed that silicate melt is attracted to the wetting surfaces of Re metal (Figure 1). Re traps are made by folding three pieces of Re foil around each other to maximize corner space as shown in Figure 2. The Re trap works similarly to vitreous carbon spheres but it uses the Re foil as a wetting surface to attract melt. The combination of the melt's affinity for the rhenium surface and an initial pressure-low draws the melt phase into the trap. This low pressure effect is probably not as significant as in the diamond aggregate experiments because the Re is much softer and unlikely to withstand pressure of 3 GPa over the run duration.

Experimentation has shown that Re does not react with molten silicates and should not affect the silicate phase equilibria in partial melting experiments. Lesher et al (2003) performed melting experiments on mantle xenolith KR4003 at 5 GPa over a range of pressures in both Re and Pt-graphite capsules. The types and modes of phases present were not affected by capsule type, and the solidus temperature did not vary. While bits of displaced Re within the charge were observed in this and other studies (e.g. Righter and

Hauri, 2006), this may simply be an artifact of polishing and was shown to have no effect on melt chemistry.

In this study the Re traps are tested for their ability to trap peridotite partial melts and keep them in chemical equilibrium with the residue. Experiments cover a range of temperatures at a pressure of 3 GPa. The following discussion includes a review of the new Re melt trap method and implications of our new melt analyses for mantle melting and the formation of OIB.

Experimental and Analytical Procedures

Starting compositions were natural peridotite xenolith KLB-1 from Kilbourne Hole, New Mexico, USA and an oxide mix, Mix KLB-1 made to approximate KLB-1. The powdered KLB-1 sample was provided by Claude Herzberg. KLB-1 was chosen as the starting mix because it is widely considered to represent bulk upper mantle fertile peridotite. Major element compositions of the starting materials are given in Table 1.

Experiments were run in graphite-lined Pt capsules. First, a Re trap was prepared by folding 3 pieces of Re foil and fitting them together into the arrangement shown in Figure 2. This configuration maximizes the number of open fold edges where melt pools are likely to form. A Re trap was placed in the bottom of a graphite inner capsule, which was then filled with peridotite powder. The graphite capsule was placed in a 4 mm Pt outer capsule, and more loose graphite powder was packed in to completely isolate the peridotite from the Pt to minimize iron loss. The open end of the capsule was coned to a point on a lathe. The capsule was kept overnight in a drying oven in order to remove water which may have adhered itself to the capsule during the loading process. Before

the experiment was performed, the capsule was welded shut, and the cone was hammered flat.

Partial melting experiments were performed in a ½" end-loaded piston cylinder apparatus using the piston-in technique. The capsule was loaded into a crushable MgO spacer, oriented such that the Re trap would be at the top end of the experiment where the temperature is warmest and the melt is likely to migrate. The MgO spacer was surrounded by a graphite furnace and a BaCO3 pressure medium. Experiments were raised to a pressure of 2.6-2.8 GPa at room temperature. Temperature was then increased to run conditions, and after pressure fluctuations from thermal expansion stopped, the pressure was brought up to 3 GPa, usually within the first hour of the experiment. The apparatus requires a pressure correction of -0.2 GPa and a temperature correction of 12 °C. Temperature was monitored using a Type D W-Re thermocouple. The fO_2 of the experiments was not buffered, but the inner graphite capsule prevented it from exceeding graphite-CO. Experiments were run for 24 hours and quenched by cutting the power. A list of experiments and run conditions is given in Table 2.

After the capsule was retrieved from the assembly, it was fixed to a brass mount with epoxy. The capsules were polished using a series of diamond or alumina pads decreasing in grit to 1 μm. Some samples were polished with 0.3 μm alumina slurry. This method facilitates phase identification of minerals under the microprobe, but often removes quenched melt material from the edges of the Re trap. A better polish for melt phase analysis was obtained with colloidal silica.

Phase identification and major element analyses were performed using the JEOL JXA-8900 microprobe at the University of Minnesota. An accelerating voltage of 15 kV

and a focused spot were used for all phases. Probe current was set to 10 nA for quenched melt analyses and 15 nA for mineral phase analyses. Count times were 10 seconds off peak and 20 seconds on peak for all oxides except Na_2O. To reduce Na loss, Na_2O counting times were 5 seconds off peak and 10 seconds on, and Na_2O was measured by the first pass of the spectrometer. Some garnets contained remnant cores, but the small volume of these cores (<1 μm in diameter) relative to the whole grain (10-20 μm diameter) was assumed to have a negligible effect on equilibrium conditions. When analyzing these garnets, care was taken to avoid unreacted cores.

A line analysis was performed across the width of a piece of a Re-foil trap in experiment A595 to look for Fe metal. The accelerating voltage was 15 kV, the spot was focused, and a beam current of 30 nA was used. The points of the scan were spaced at 1 μm intervals beginning at the bottom edge of the foil segment.

Results

Mineral and quenched melt compositions determined by microprobe analysis are given in Table 3. Mineral phases present (Table 2) were olivine + orthopyroxene + clinopyroxene ± garnet. Garnet was present only in runs A593 and A598 (1490 °C and 1470 °C respectively). Garnets in A598 had large unreacted spinel cores suggesting an incomplete approach to equilibrium. Melt analyses from A598 are not included in the study for this reason. The melt fractions and proportions of mineral phases (Table 2) were determined by least sum of square residuals mass balance calculation. Oxide compositions determined by microprobe analysis of melt and mineral phases are located in Tables 3-7.

Quenched Liquid

Experiments produced heterogeneous quenched melt pools within the Re traps, and traps often included crystal phases as well (Fig. 3). The presence of the minerals and the heterogeneous nature of the quench pools presented a challenge for analysis. First, crystal-free areas of the glass had to be located. Often these were small areas (Figure 3) ~5 μm diameter. These small pools could not be analyzed by defocused beam, so a large number of spot analyses were needed to provide a meaningful average (Table 3). Some experiments had to be polished a second time to expose a new layer of the trap in order to acquire a sufficient number of spots. A colloidal silica polishing step was added because initial analyses returned low totals.

The temperature-melt fraction relationship has been plotted in Figure 4. It agrees well with other peridotite melting studies. The oxide compositions of the melts are given in Table 3. In Figure 5 these data are plotted against other peridotite melting data. A comparison of these data is included in the following discussion.

Olivine

Olivine is the dominant mineral phase in all experiments. Olivine compositions display a linear increase in Mg# with increasing melt fraction (Figure 6, Table 4) that fits well with the olivines from Walter (1998) and Hirose and Kushiro (1993). The SiO_2 and MgO contents of olivines decrease with decreasing melt fraction, and FeO* increases. Most of the oxide trends show good agreement with previous measurements at higher melt fractions. The differences seen in Al_2O_3 and CaO contents may be due to the presence of garnet phases in the lowest melt fraction experiments.

Pyroxenes

Orthopyroxene is the next most common mineral phase after olivine. Like olivine, orthopyroxene increases in Mg# with increasing melt fraction in agreement with Walter (1998). SiO_2 in opx increases with melt fraction above ~15% melt (Table 5). Clinopyroxene, which decreases in mode approaching complete consumption around 1530 °C, increases in MgO, SiO_2, and Mg# with increasing melt fraction while CaO decreases (Table 6).

Garnet

Garnet is only present in A593 and A598 at temperatures of 1490° and 1470°. In both experiments garnets exhibit bright (spinel-rich) cores in BSE images. Cores in A593 garnets were considered to have no significant effect on analyses or approach to equilibrium as care was taken to analyze rims and the cores were small (<1 μm diameter) compared with size of the garnet grains (~ 10-20 μm diameter) accounting for a fraction of grain volumes. Garnet analyses are listed in Table 7. Cores in A598 were much larger and probably significantly affected approach to equilibrium. Garnet is the only phase that is consumed over the temperature range we have examined, and a discussion of the effects of its presence is included in the following section.

Discussion

Comparison of experimentally determined melts and OIB

Melt phase oxide compositions versus melt fraction are plotted in Figure 5 along with 3 GPa measurements of KLB-1 from Hirose and Kushiro (1993) and KR4003 from Walter (1998) to compare our results with trends established at higher melt fractions. Our data extend into the melt fraction range of these earlier experiments and show good agreement for most of the oxides, especially TiO_2, Al_2O_3, Cr_2O_3, MnO, MgO, and Na_2O.

The incompatible oxide TiO_2 shows an increasingly high concentration at lower extents of melting. The implication is that TiO_2 concentrations at very low (~1%) melt fractions maybe much higher than previous models would suggest. Since some recent studies have attempted to use TiO_2 concentrations in OIB as a proxy for extent of melting (Prytulak and Elliott, 2007), it is important that this trend is explored to even lower melt fractions.

The incompatible alkali, Na_2O, also shows an increasing trend at lower melt fractions. K_2O in KLB-1 melts is much lower than in KR4003 because the starting materials differ so greatly in K_2O. Interestingly, the KLB-1 experiments of Hirose and Kushiro (1993) produced melts with significantly greater K_2O.

Al_2O_3 shows an increasing trend at lower melt fractions except for the two lowest melt fraction experiments. These two outline a trend of decreasing Al_2O_3 with decreasing extent of melting. These are the only two melts that equilibrated with garnet, the likely source of the trend. More experiments in the temperature region of the garnet-out reaction will better define the turnover temperature. The turnover trend is also seen in our CaO measurements and may also be due to the presence of garnet.

There are significant differences in weight percent CaO and FeO* between this and previous studies. CaO contents of our melts are high in comparison to Walter (1998) and Hirose and Kushiro (1993). It is not obvious why this should be so. It may be due to an over-sampling of the cpx component of the quenched melts, or it may be an effect of quenching melts in close proximity to the crystalline residue. The FeO* content of our melts are also low compared with other peridotite partial melting studies.

Low Fe in the melt might be caused be Fe-loss, either to the Pt capsule or to the Re trap, but this is unlikely. Examination of the Mg# of olivines in these experiments (figure 6) shows Mg# to be consistent with mineral phases in other experiments. Significant Fe-loss should result in anomalously high Mg# in mineral phases. Also, Re is not expected to alloy with Fe (Lesher et al., 2003). To check this assumption a microprobe line-scan for Fe across a section of Re foil in contact with silicate phases was performed. The results of the scan are given in Figure 7 and Table 8. Fe is elevated at the edges of the foil because of sampling of the adjacent silicate phases. Most of the points inside the foil give iron contents not significantly greater than zero. One small peak (<0.20) is centered at 12 μm. This is still a tiny amount of Fe, and the quick diffusion rate of metals suggest that this peak may not be Fe alloyed with the Re but sampling of silicate material deeper in the capsule. Fe may also have been lost to the outer Pt capsule, but there is no evidence of a connection through the ~1 mm-thick walls of the inner graphite capsules.

Since melting associated with OIB generation occurs at the base of the oceanic lithosphere around a depth of 100 km and pressure of 3 GPa, our data should provide insight into the role of peridotite in OIB formation. In Figure 8 experimental melt compositions are shown with OIB from eight localities, Austral-Cook, Azores, Canary, Cape Verde, Galapagos, Hawaii, Pitcairn-Gambier, and Society, plotted as oxides versus MgO. MgO serves as a good proxy for melt fraction in our experimental set with the exception of the Mix KLB-1 experiment, which has a slightly different starting composition and so is not suited for direct comparison.

While these results do not support the possibility of a peridotite-only OIB source, there are signs that peridotite may heavily influence the bulk chemistry. SiO_2 and MnO fit into the bulk of OIB data at ~14% MgO. Some trends, especially Na_2O and TiO_2 seem likely to intersect the OIB cloud if they are extended to lower melt fractions. However, to suggest that all of these trends will fall in the OIB cloud at very low melt fractions (>0.02) would be overly-optimistic.

Despite the decreasing trend of Al_2O_3 in the presence of garnet, it appears that peridotite melts from our experiments are too rich in Al_2O_3 to be the sole source of OIB. CaO is also too high, and FeO* is too low.

Effectiveness of the Re melt traps

The Re melt trap provided mixed results. While not every experimental attempt produced measurable quenched melt, the success rate was high once the fold geometry was changed to maximize fold corners. The Re traps are easy to construct and polish easily with either alumina or diamond polishing agents and thus avoid the polishing difficulties of the diamond aggregate method. Although, it is often difficult to find large pools of melt for analysis, and may require several polishing steps. This problem became severe enough at a melt fraction of 0.059 that it seems unlikely that experiments at lower melt fractions would be able to provide melt pools large enough for analysis.

It is unclear if Re traps would be of use at pressures >3 GPa. Unlike vitreous carbon spheres, Re is stable at 3 GPa; however, it is unclear whether the Re traps suffer from the formation of pressure gradients similar to those present in diamond aggregate traps. Silicate melt is certainly attracted to Re metal as a wetting surface, but there may be some influence of a negative pressure gradient that is partly responsible for trapping of

melt. Re is a relatively hard metal, but it is easily worked by hand. It may be that at pressures much higher than 3 GPa Re traps will fail to withstand loading pressure and may not accommodate any melt within the folds of the trap.

Because the initial melt that enters a melt trap is not the equilibrium melt, the hope is that this initial liquid will continue to equilibrate by diffusion with the rest of the charge throughout the duration of the experiment. There is another way that this equilibration can take place: crystallization from the melt. In many of the experiments crystalline phases were present in the melt traps. It is difficult to determine whether these minerals were introduced to the trap during loading of the peridotite powder, or if they grew in situ. Regardless, their presence is a problem for analysis. An important reason to build melt traps is to isolate melts from mineral phases that serve as potential quench nucleation sites. The heterogeneous character of the melts may have been a result of their close proximity to minerals inside the melt traps.

Despite its problems, we were able to use Re traps to produce peridotite melts that agreed somewhat with previous data and extended our knowledge of the chemical character of these melts to crucial lower melt fractions. The heterogeneous nature of our melts coupled with the disagreement with previous studies in both CaO and FeO* contents, suggest that the melts produced in these experiments are not actually 3 GPa peridotite equilibrium melts. The method seems to have value as a quick way to obtain approximate melt compositions, but at this stage of development more rigorous experimental methods, such as iterative sandwich experiments, or better analysis techniques for quenched melts may be necessary to determine precisely the composition of these low-degree peridotite melts.

References

Baker MB, Stolper EM (1994) Determining the composition of high-pressure mantle melts using diamond aggregates. Geochimica Et Cosmochimica Acta 58(13):2811-2827

Chauvel C, Hofmann AW, Vidal P (1992) Himu Em - The French-Polynesian Connection. Earth And Planetary Science Letters 110(1-4):99-119

Dasgupta R, Hirschmann MM, Smith ND (2007) Partial melting experiments of peridotite CO_2 at 3 GPa and genesis of alkalic ocean island basalts. J. Petrol. 48(11):2093-2124

Falloon TJ, Green DH (1987) Anhydrous partial melting of MORB pyrolite and other peridotite compositions at 10 kbar: implications for the origin of primitive MORB glasses. Mineralogy and Petrology 37:181-219

Falloon TJ, Green DH, Danyushevsky LV, Faul UH (1999) Peridotite melting at 1.0 and 1.5 GPa: an experimental evaluation of techniques using diamond aggregates and mineral mixes for determination of near-solidus melts. J. Petrol. 40(9):1343-1375

Falloon TJ, Green DH, Oneill HSC, Ballhaus CG (1996) Quest for low-degree mantle melts. Nature 381(6580):285-285

Hauri EH (1996) Major-element variability in the Hawaiian mantle plume. Nature 382:415-419

Hirose K (1997a) Melting experiments on lherzolite KLB-1 under hydrous conditions and generation of high-magnesian andesitic melts. Geology 25(1):42-44

Hirose K (1997b) Partial melt compositions of carbonated peridotite at 3 GPa and role of

CO_2 in alkali-basalt magma generation. Geophysical Research Letters 24(22):2837-2840

Hirose K, Kawamoto T (1995) Hydrous partial melting of lherzolite at 1 GPa: The effect of H_2O on the genesis of basaltic magmas. Earth And Planetary Science Letters 133:463-473

Hirose K, Kushiro I (1993) Partial melting of dry peridotites at high-pressures – determination of compositions of melts segregated from peridotite using aggregates of diamond. Earth And Planetary Science Letters 114(4):477-489

Hirschmann MM (2000) Mantle solidus: experimental constraints and the effects of peridotite composition. Geochemistry Geophysics Geosystems 1

Hirschmann MM, Dasgupta R (2007) A modified iterative sandwich method for determination of near-solidus partial melt compositions. I. Theoretical considerations. Contributions To Mineralogy And Petrology 154(6):635-645

Hirschmann MM, Kogiso T, Baker MB, Stolper EM (2003) Alkalic magmas generated by partial melting of garnet pyroxenite. Geology 31(6):481-484

Hofmann AW (1988) Chemical differentiation of the Earth: the relationship between mantle, continental crust, and oceanic crust. Earth And Planetary Science Letters 90:297-314

Hofmann AW (1997) Mantle geochemistry: the message from oceanic volcanism. Nature 385:219-229

Hofmann AW, White WM (1982) Mantle plumes from ancient oceanic-crust. Earth And Planetary Science Letters 57(2):421-436

Johnston AD (1986) Anhydrous P---T phase relations of near-primary high-alumina

basalt from the South Sandwich Islands. Contributions To Mineralogy and Petrology 92:368-382

Kogiso T, Hirschmann MM (2001) Experimental study of clinopyroxenite partial melting and the origin of ultra-calcic melt inclusions. Contributions To Mineralogy And Petrology 142:347-360

Kogiso T, Hirschmann MM, Frost DJ (2003) High-pressure partial melting of garnet pyroxenite: possible mafic lithologies in the source of ocean island basalts. Earth And Planetary Science Letters 216(4):603-617

Laporte D, Toplis MJ, Seyler M, Devidal JL (2004) A new experimental technique for extracting liquids from peridotite at very low degrees of melting: application to partial melting of depleted peridotite. Contributions To Mineralogy And Petrology 146(4):463-484

Lesher CE, Pickering-Witter J, Baxter G, Walter M (2003) Melting of garnet peridotite: Effects of capsules and thermocouples, and implications for the high-pressure mantle solidus. American Mineralogist 88(8-9):1181-1189

Mysen BO, Kushiro I (1977) Compositional Variations Of Coexisting Phases With Degree Of Melting Of Peridotite In Upper Mantle. American Mineralogist 62(9-10):843-856

Pertermann M, Hirschmann MM (2003) Anhydrous partial melting experiments on MORB-like eclogite: Phase relations, phase compositions and mineral-melt partitioning of major elements at 2-3 GPa. J. Petrol. 44(12):2173-2201

Pickering-Witter J, Johnston AD (2000) The effects of variable bulk composition on the melting systematics of fertile peridotitic assemblages. Contributions To

Mineralogy And Petrology 140(2):190-211

Prytulak J, Elliott T (2007) TiO_2 enrichment in ocean island basalts. Earth And Planetary Science Letters 263(3-4):388-403

Righter K, Hauri EH (1998) Compatibility of rhenium in garnet during mantle melting and magma genesis. Science 280(5370):1737-1741

Robinson JAC, Wood BJ, Blundy JD (1998) The beginning of melting of fertile and depleted peridotite at 1.5 GPa. Earth and Planetary Science Letters 155(1-2):97-111

Stolper E (1980) A phase diagram for mid-ocean ridge basalts: preliminary results and implications for petrogenesis. Contributions To Mineralogy And Petrology 74:13-27

Takahashi E, Kushiro I (1983) Melting of a dry peridotite at high pressures and basalt magma genesis. American Mineralogist 68: 859-879

Takahashi E, Nakajima K (2002) Melting processes in the Hawaiian plume: and experimental study. Geophysial Monograph 128:403-418

Walter MJ (1998) Melting of garnet peridotite and the origin of komatiite and depleted lithosphere. J. Petrol. 39(1):29-60

Wasylenki LE, Baker MB, Kent AJR, Stolper EM (2003) Near-solidus melting of the shallow upper mantle: Partial melting experiments on depleted peridotite. J. Petrol. 44(7):1163-1191

Yasuda A, Fujii T, Kurita K (1994) Melting phase relations of an anhydrous mid-ocean ridge basalt from 3 to 20 GPa; implications for the behavior of subducted oceanic crust in the mantle. Journal of Geophysical Research 99:9401-9414

Yaxley GM, Green DH (1998) Reactions between eclogite and peridotite: mantle refertilization by subduction of oceanic crust. Schweizerische Mineralogische und Petrographische Mitteilungen 78:243-255

Yaxley GM, Sobolev AV (2007) High-pressure partial melting of gabbro and its role in the Hawaiian magma source. Contributions To Mineralogy And Petrology 154(4):371-383

Zindler A, Hart S (1986) Chemical geodynamics. Annu. Rev. Earth Planet. Sci. 14:493-571

Figure 1. A basalt melting experiment performed in a Re capsule. Instead of pressure welding, the folds have filled with basaltic melt. The fold edges hold open triangular melt pockets with large melt pools. This served as the model for the Re trap design.

Figure 2. Schematic of the experimental capsule design showing the Re trap at the top of the capsule where melt tends to coalesce. The trap is made of three pieces of Re foil folded as shown to maximize the number of exposed fold hinges, which provide large melt-filled areas.

Figure 3. Back-scattered electron images taken with a JEOL JXA-8900 microprobe. (A) Experiment B197 showing a particularly large melt pool in the Re trap. The heterogeneous nature of the quenched melt phase is evidenced by the lighter colored streaks in the melt pool. Darker mineral phases can be seen to the far left side of the Re trap. These phases may be the result of dry powder entering the trap during capsule loading or may be the result of crystallization from the liquid during the run. (B) This melt trap from experiment A595 is more typical of the texture observed. A small portion of the melt in the trap can be analyzed by electron beam, but many of the folds are closed too tightly to be analyzed. The quenched liquid phase displays heterogeneity in this image as well.

Figure 4. Temperature (T) plotted against melt fraction (F) showing experiments from this study and 3-GPa peridotite partial melting experiments of KR4003 from Walter (1998) and KLB-1 from Hirose and Kushiro (1993). Melt fractions from Hirose and

Kushiro (1993) shown are recalculated from the bulk partition coefficient of Na_2O in the glass phase as in Hirschmann (2000). Original published melt fractions were calculated based on a treatment of Na_2O as a perfectly incompatible component. The new KLB-1 and Mix KLB-1 experiments fit linearly with other peridotite melting experiments.

Figure 5. Oxide concentrations of the quenched melt phase plotted against melt fraction (F). 3-GPa melt analyses from Walter (1998) and Hirose and Kushiro (1993) are included for comparison. Melt fractions from Hirose and Kushiro (1993) are recalculated as in Figure 4. Changes in Al_2O_3 and CaO concentrations at low melt fraction may be the result of the presence of garnet in the two lowest F experiments. While many of the oxide-melt fraction trends are in good agreement with previous studies, it is notable that CaO is consistently higher and FeO* is consistently lower than in previous studies.

Figure 6. Mg# and oxide concentrations of olivine plotted against melt fraction (F). Data from Walter (1998) and Hirose and Kushiro (1993) are included for comparison. Melt fractions from Hirose and Kushiro (1993) are recalculated as in Figure 4. The continuation of the trend in Mg#, established by previous works, to lower values at low melt fractions is particularly strong evidence that there was no significant iron-loss during the experimental run. Oxide concentrations show good agreement with higher melt fraction analyses from previous studies.

Figure 7. Microprobe line analysis across the width of a piece of a rhenium foil trap from experiment A595. The distance in μm is from the bottom edge of the Re foil. The

elevated Fe values at the margins are due to sampling the adjacent silicate material. Aside from the small peak centered at 12 μm from the starting point, Fe concentration doesn't vary significantly from zero. The small peak may be due to sampling silicate material beneath the surface..

Figure 8. Harker plots displaying our peridotite partial melts with OIB analyses collected from the GEOROC database. While some of the trends compare favorably with OIB (TiO_2, Al_2O_3, Na_2O), few of the oxide concentrations plot within the OIB array. The low-degree peridotite melts determined in this study cannot be the sole source of OIB magmas.

Table 1: Major oxide compositions of starting materials and similar peridotite for comparison

	KLB-1[a]	Oxide mix	KR4003[b]
SiO2	44.84	44.92	44.90
TiO2	0.11	0.16	0.16
Al2O3	3.51	3.92	4.26
Cr2O3	0.32	0.28	0.41
FeO	8.20	8.09	8.02
MnO	0.12	0.12	0.13
MgO	39.52	38.76	37.30
CaO	3.07	3.79	3.45
Na2O	0.30	0.30	0.22
K2O	0.02	0.03	0.09
Total	100.01	100.36	98.94

a – from Davis et al, 2008

b – from Walter, 1998

Table 2: List of experiments and run conditions

Experiment name	starting composition	T (°C)	P (Gpa)	t (hours)	phases (modes)
A591	KLB-1	1510	3	24	liq (14.7), ol (60.8), opx (19.2), cpx (5.2)
A593	KLB-1	1490	3	24	liq (5.9), ol (62.0), opx (13.4), cpx (15.4), gt (3.2)
A595	KLB-1	1530	3	24	liq (22.3), ol (61.1), opx (16.6), cpx (0)
A597	KLB-1	1510	3	24	liq (15.9), ol (60.3), opx (21.9), cpx (2.0)
A598	KLB-1	1470	3	24	liq, ol, opx, cpx, gt, spn*
A631	oxide mix	1500	3	24	liq (23.5), ol (59.5), opx (11.6), cpx (5.4)

Phase abbreviations are as follows: liq=quenched melt, ol=olivine, opx=orthopyroxene, cpx=clinopyroxene, gt=garnet, spn=spinel

Modes calculated by least sum of square residuals mass balance

* - spinel exists as unreacted cores in garnet

Table 3: Quenched melt analyses

Experiment	A591	err	A593	err	A595	err	A597	err	B197	err
N	18		11		9		21		14	
SiO2	47.39	0.19	47.40	0.77	48.37	0.24	47.09	0.24	47.94	0.62
TiO2	0.50	0.03	1.03	0.23	0.41	0.02	0.55	0.03	1.54	0.16
Al2O3	12.95	0.21	13.44	0.67	11.22	0.20	13.68	0.27	12.19	0.33
Cr2O3	0.43	0.03	0.24	0.04	0.44	0.03	0.37	0.03	0.20	0.03
FeO*	6.57	0.20	7.92	0.52	7.57	0.27	6.64	0.11	7.28	0.46
MnO	0.14	0.01	0.15	0.01	0.17	0.01	0.17	0.01	0.17	0.00
MgO	17.41	0.31	14.71	1.00	19.28	0.44	16.15	0.33	17.71	0.49
CaO	13.65	0.21	13.35	0.43	11.42	0.38	14.29	0.19	11.68	0.45
Na2O	0.87	0.04	1.20	0.15	0.75	0.05	0.84	0.03	1.20	0.21
K2O	0.03	0.00	0.02	0.01	0.02	0.01	0.02	0.00	0.06	0.03
Total	99.94		99.47		99.65		99.81		99.97	
Mg#	82.5		76.8		81.9		81.3		81.3	

Errors given are deviation of the mean defined as: standard deviation/√n

Table 4: Olivine Analyses

Experiment	A591	s.d.	A593	s.d.	A595	s.d.	A597	s.d.	B197	s.d.
N	14		11		15		17		9	
SiO2	40.43	0.09	39.66	0.30	40.87	0.14	40.55	0.14	40.66	0.15
TiO2	0.01	0.02	0.01	0.01	0.01	0.01	-0.01	0.02	0.01	0.01
Al2O3	0.19	0.01	0.18	0.02	0.17	0.01	0.17	0.02	0.17	0.03
Cr2O3	0.12	0.02	0.13	0.03	0.18	0.01	0.14	0.02	0.06	0.02
FeO	9.43	0.09	9.84	0.06	9.12	0.13	9.21	0.12	9.58	0.10
MnO	0.13	0.03	0.13	0.02	0.12	0.02	0.12	0.02	0.13	0.03
MgO	48.71	0.21	48.96	0.20	49.19	0.22	49.13	0.22	48.43	0.15
CaO	0.29	0.02	0.27	0.02	0.29	0.02	0.29	0.03	0.25	0.02
Na2O	0.03	0.01	0.02	0.01	0.02	0.01	0.02	0.01	0.02	0.02
K2O	0.02	0.01	0.02	0.01	0.02	0.01	0.02	0.01	0.02	0.01
Total	99.34		99.21		99.99		99.64		99.33	
Mg#	90.2		89.9		90.6		90.5		90.0	

Table 5: Orthopyroxene Analyses

Experiment	A591	s.d.	A593	s.d.	A595	s.d.	A597	s.d.	B197	s.d.
N	14		15		13		17		11	
SiO2	53.97	0.48	53.91	0.43	54.30	0.20	53.85	0.28	54.38	0.22
TiO2	0.07	0.02	0.09	0.04	0.04	0.02	0.06	0.02	0.14	0.02
Al2O3	6.27	0.46	5.94	0.48	5.49	0.22	5.75	0.19	5.61	0.13
Cr2O3	0.68	0.11	0.59	0.11	0.70	0.06	0.72	0.06	0.38	0.03
FeO	5.70	0.10	5.79	0.10	5.42	0.09	5.53	0.07	5.62	0.06
MnO	0.11	0.02	0.12	0.02	0.12	0.02	0.10	0.02	0.12	0.02
MgO	31.07	0.57	30.88	0.76	31.09	0.46	31.37	0.34	31.65	0.15
CaO	2.13	0.41	2.04	0.50	2.30	0.30	2.31	0.26	2.21	0.06
Na2O	0.16	0.03	0.19	0.05	0.15	0.03	0.15	0.02	0.18	0.03
K2O	0.01	0.01	0.02	0.01	0.02	0.01	0.02	0.01	0.02	0.01
Total	100.16		99.55		99.59		99.86		100.31	
Mg#	90.7		90.5		91.1		91.0		90.9	

Table 6: Clinopyroxene Analyses

Experiment	A591	s.d.	A593	s.d.	A595	s.d.	A597	s.d.	B197	s.d.
N	16		16		22		21		13	
SiO2	52.68	0.29	52.44	0.31	53.53	0.36	53.03	0.39	53.52	0.37
TiO2	0.10	0.02	0.10	0.04	0.07	0.01	0.08	0.02	0.21	0.02
Al2O3	6.90	0.21	6.81	0.35	5.61	0.23	6.19	0.29	5.92	0.11
Cr2O3	0.83	0.04	0.80	0.07	0.82	0.04	0.86	0.03	0.43	0.03
FeO	5.12	0.09	5.01	0.13	5.04	0.13	5.01	0.13	4.92	0.12
MnO	0.12	0.02	0.14	0.02	0.12	0.02	0.13	0.02	0.13	0.02
MgO	23.35	0.27	22.93	0.39	24.88	0.49	23.90	0.43	23.57	0.37
CaO	10.14	0.24	10.80	0.30	9.74	0.37	10.54	0.40	11.10	0.39
Na2O	0.59	0.03	0.66	0.04	0.47	0.04	0.55	0.06	0.67	0.04
K2O	0.02	0.01	0.02	0.01	0.02	0.01	0.02	0.00	0.02	0.01
Total	99.85		99.68		100.31		100.31		100.48	
Mg#	89.0		89.1		89.8		89.5		89.5	

Table 7: Garnet Analyses

Experiment	A593	s.d.	B197	s.d.
N	12		11	
SiO2	42.01	0.12	42.46	0.24
TiO2	0.20	0.03	0.37	0.02
Al2O3	22.94	0.22	23.25	0.28
Cr2O3	1.86	0.11	1.01	0.06
FeO*	6.20	0.10	6.48	0.10
MnO	0.18	0.02	0.20	0.01
MgO	20.80	0.15	21.19	0.08
CaO	5.23	0.19	5.12	0.11
Na2O	0.02	0.01	0.02	0.01
K2O	0.01	0.01	0.02	0.01
Total	99.49		100.12	
Mg#	85.7		85.4	

Analyses taken with care to avoid unreacted cores

Table 8: Line analysis across width of Re foil trap from experiment A595

Distance from bottom edge of foil (μm)	Fe	Re[1]	Total
1	0.118	99.882	100
2	0.031	99.969	100
3	0.032	99.968	100
4	-0.004	100.004	100
5	0.026	99.974	100
6	-0.028	100.028	100
7	0.027	99.973	100
8	-0.015	100.015	100
9	0.024	99.976	100
10	0.01	99.99	100
11	0.056	99.944	100
12	0.169	99.831	100
13	0.143	99.857	100
14	0.07	99.93	100
15	0.004	99.996	100
16	-0.022	100.022	100
17	-0.013	100.013	100
18	0.033	99.967	100
19	0.239	99.761	100
20	2.626	97.374	100

1 - Calculated by subtraction

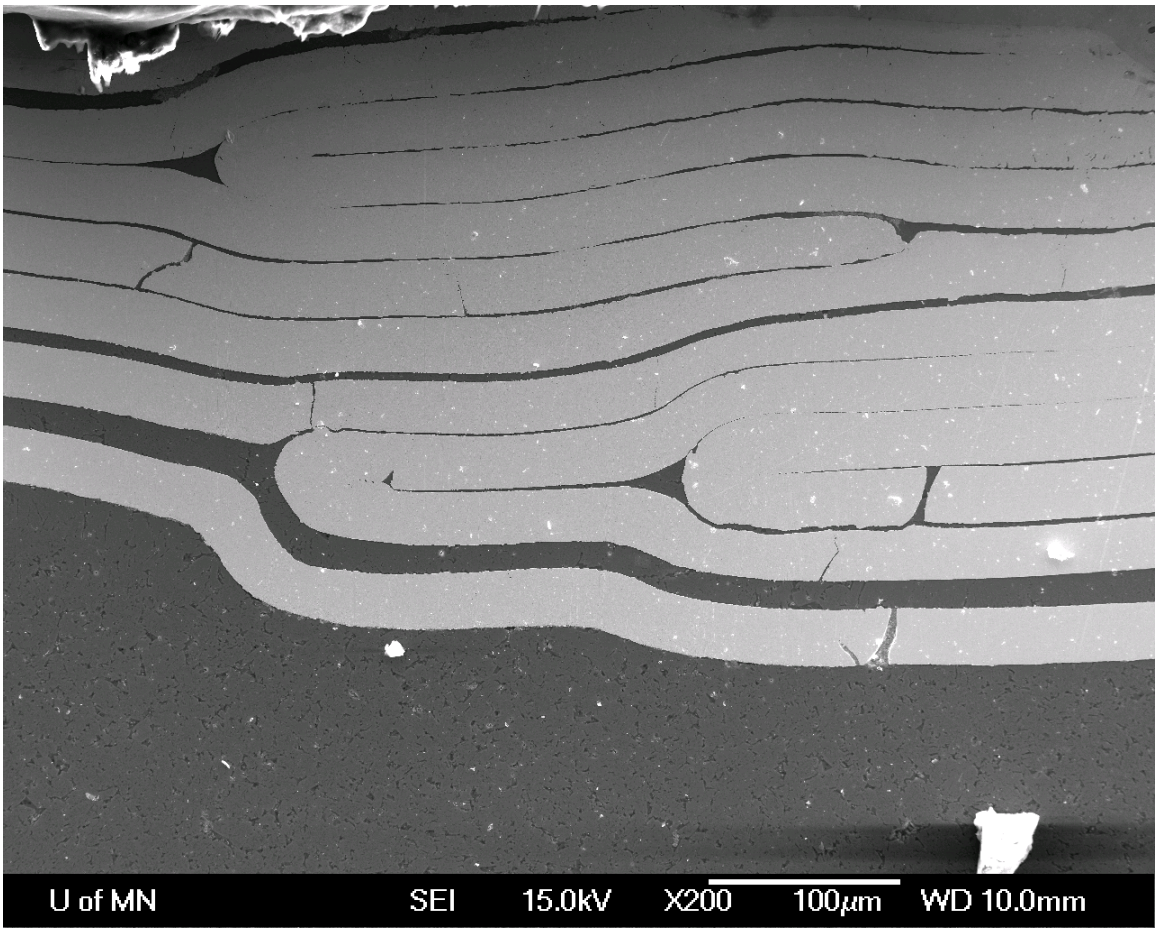

Figure 1

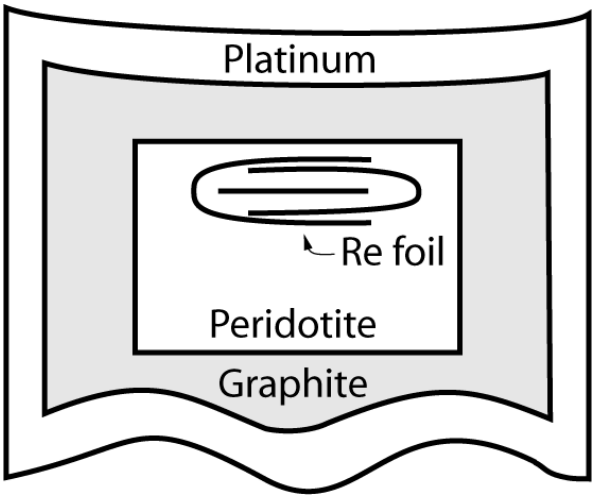

Figure 2

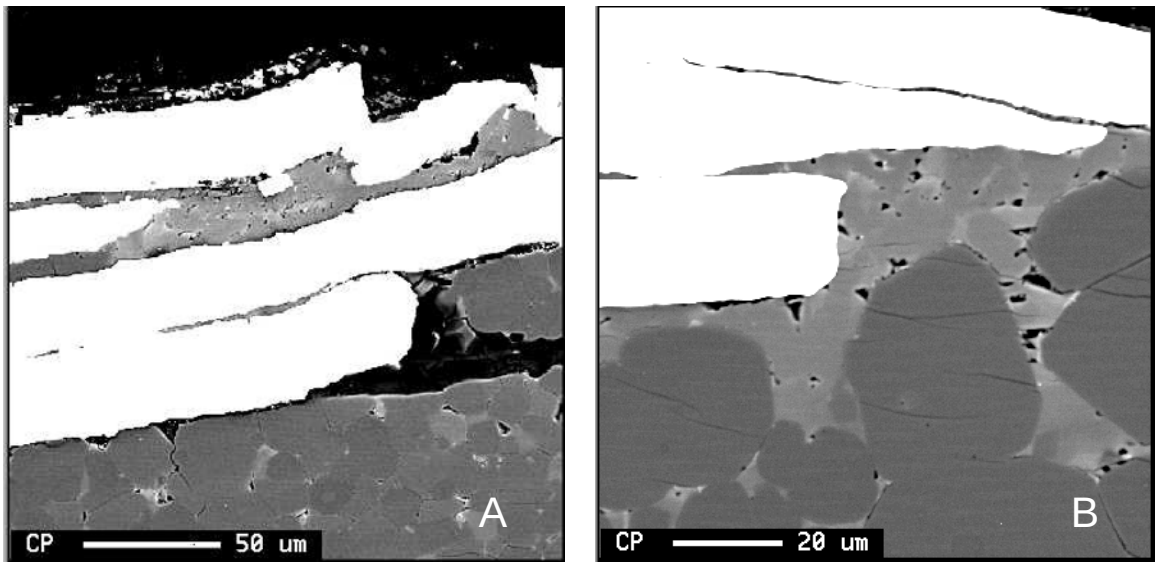

Figure 3

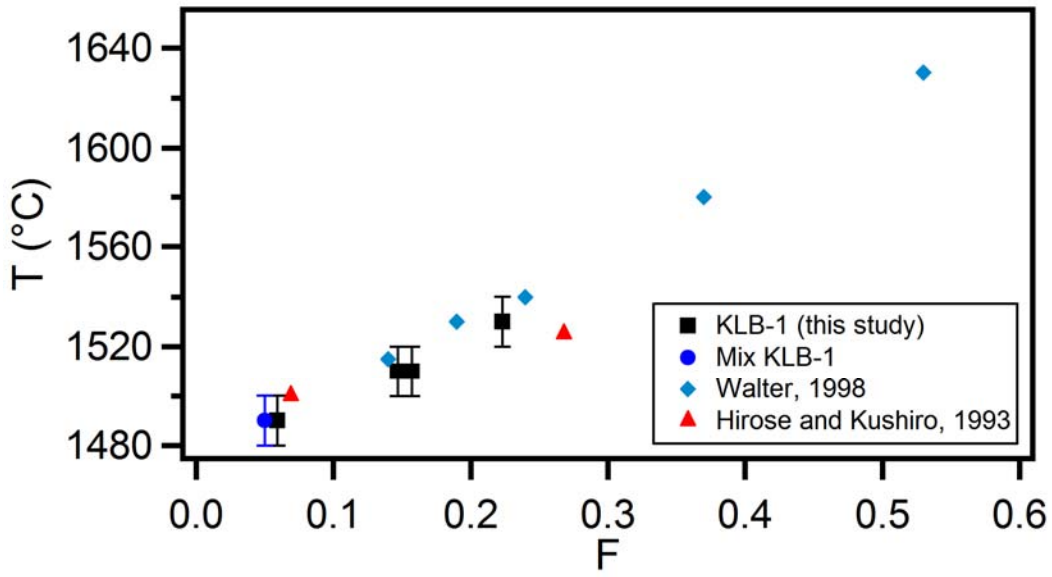

Figure 4

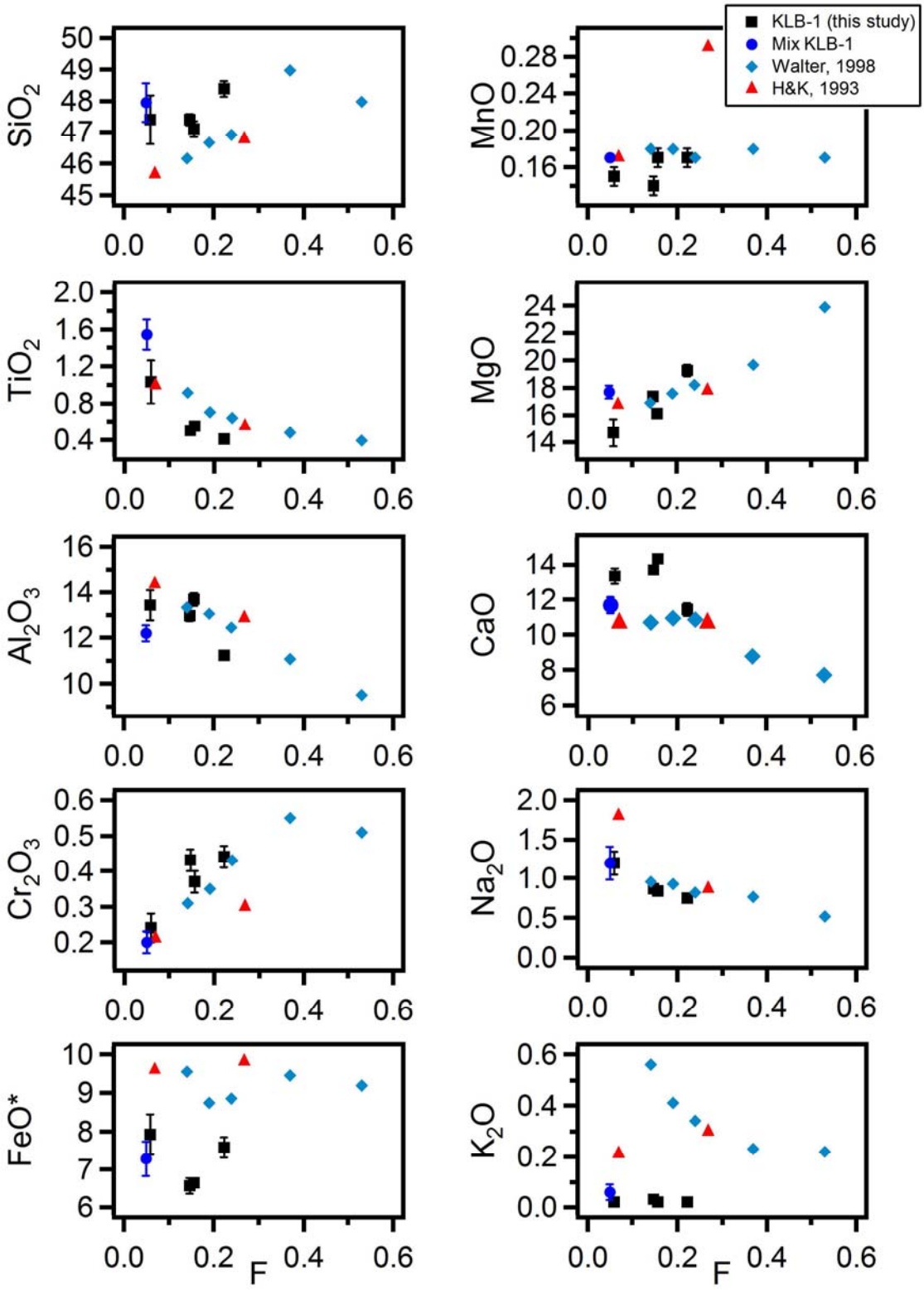
KLB-1 (this study)
Mix KLB-1
Walter, 1998
H&K, 1993
SiO2
TiO2
Al2O3
Cr2O3
FeO*
MnO
MgO
CaO
Na2O
K2O
F
F

Figure 5

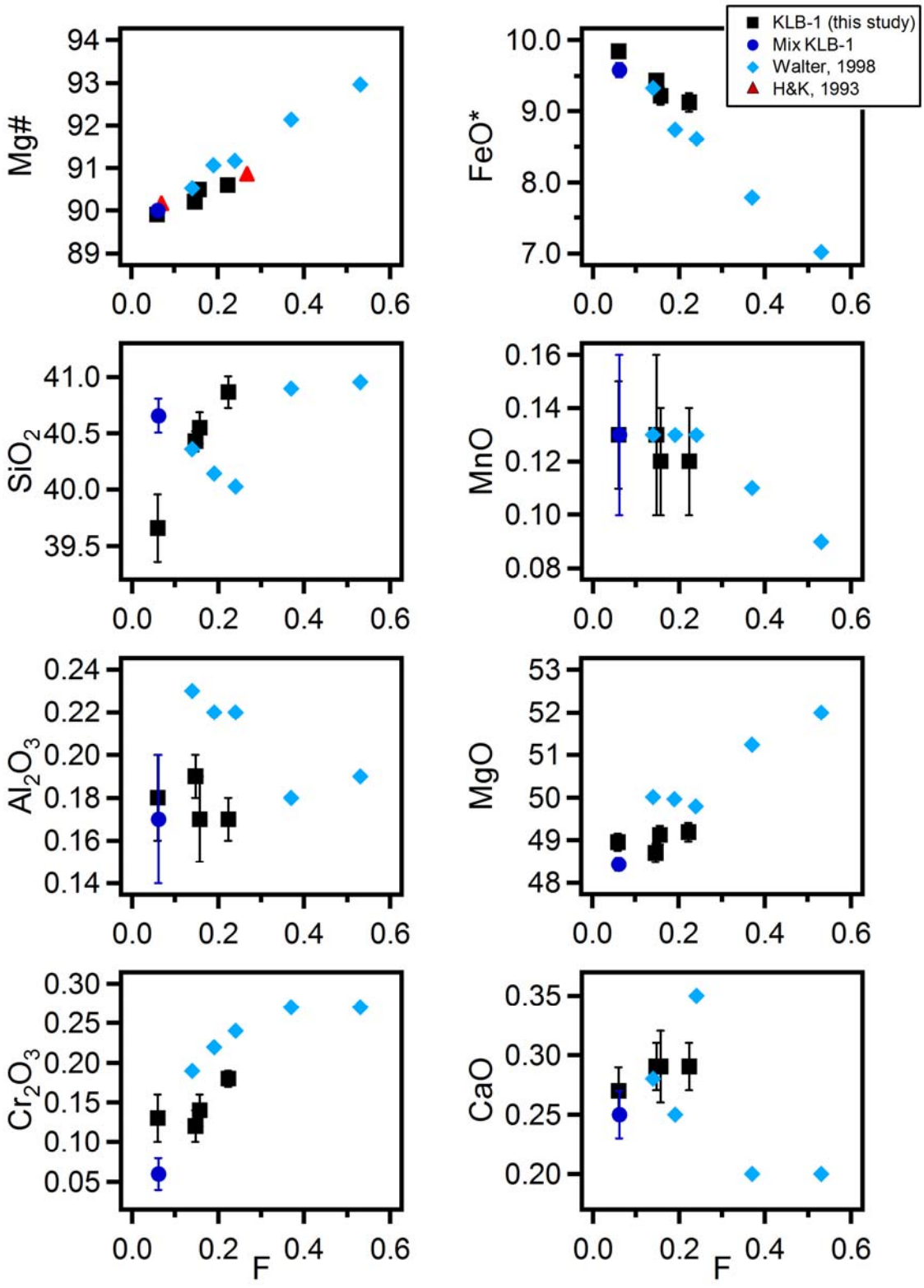
KLB-1 (this study)
Mix KLB-1
Walter, 1998
H&K, 1993
Mg#
FeO*
SiO2
MnO
Al2O3
MgO
Cr2O3
CaO
F
F

Figure 6

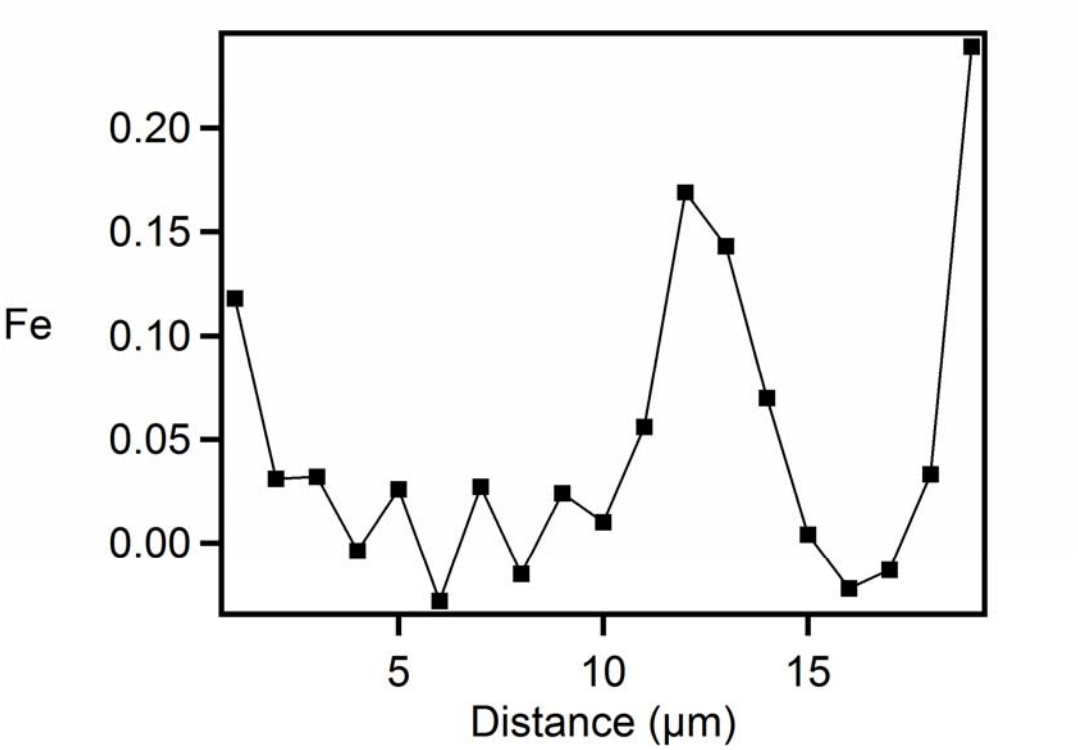

Figure 7

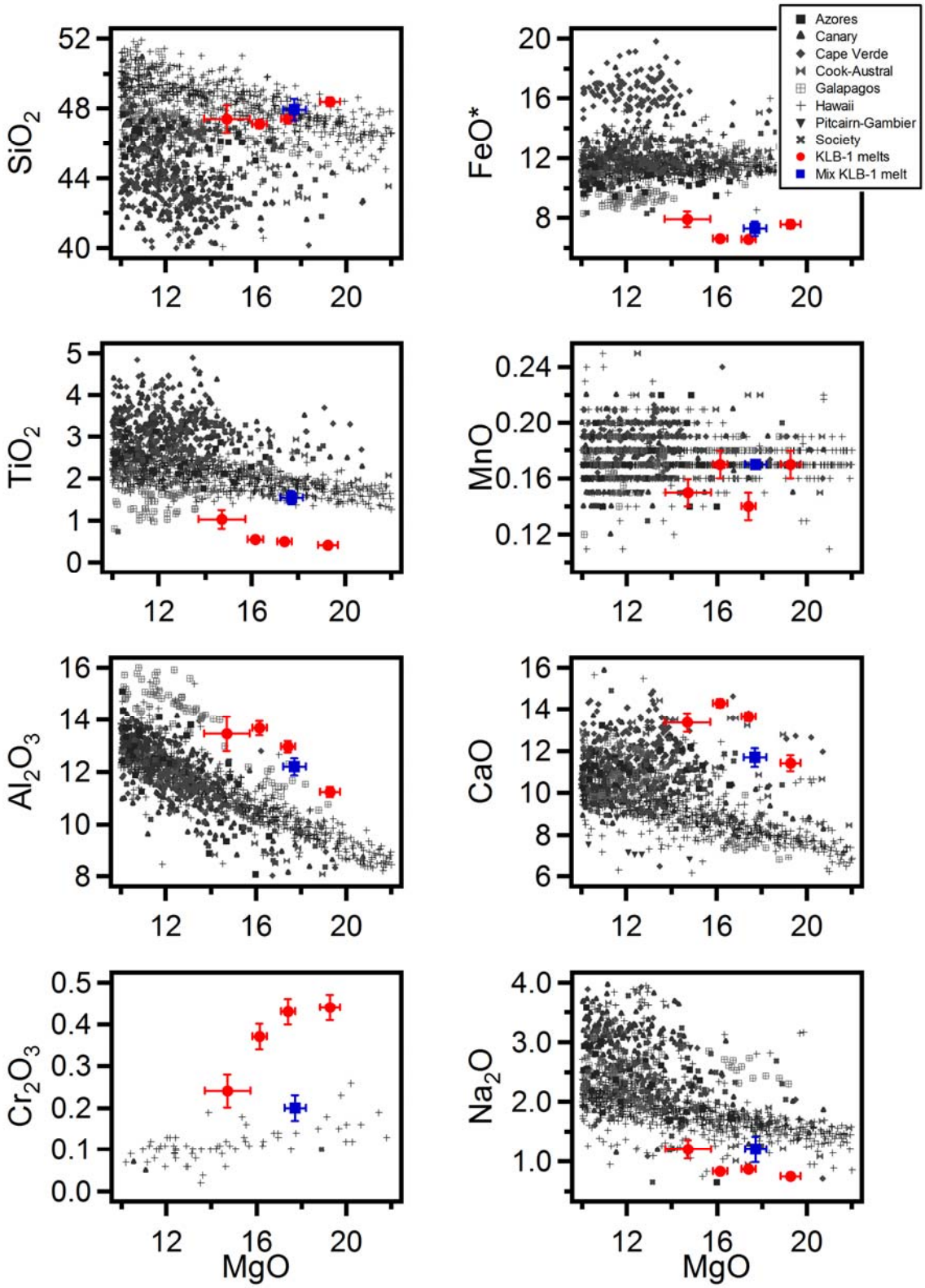
SiO2
FeO*
TiO2
MnO
Al2O3
CaO
Cr2O3
Na2O
MgO
MgO
Azores
Canary
Cape Verde
Cook-Austral
Galapagos
Hawaii
Pitcairn-Gambier
Society
KLB-1 melts
Mix KLB-1 melt

Figure 8